# Integrated Precision Landing Performance and Technology Assessments of a Human-Scale Mars Lander Using a Generalized Simulation Framework

Rafael A. Lugo,<sup>1</sup> Alicia Dwyer Cianciolo,<sup>2</sup> R. Anthony Williams,<sup>3</sup> and Soumyo Dutta<sup>4</sup>

NASA Langley Research Center, Hampton, Virginia, 23681, USA

Richard W. Powell<sup>5</sup>

Analytical Mechanics Associates, Hampton, Virginia, 23666, USA

Po-Ting Chen<sup>6</sup>

Jet Propulsion Laboratory, Pasadena, California, 91109, USA

Human-scale missions to Mars will likely require multiple landers delivered precisely to designated locations. The current NASA human Mars reference architecture assumes delivery of three 25 t payloads from a 1- or 5-Sol orbit to the surface with a landing precision of 50 m to ensure logistics are located near the habitat. While initial navigation estimates improve with on-orbit ground tracking, errors increase during post-deorbit coast. Likewise, Mars atmospheric variability and forecasting uncertainty means that the entry vehicle guidance, navigation, and control systems must be robust to accommodate landing during any time of day or Mars year, including during dust storms. Precision landing technologies are currently being assessed to determine if onboard navigation sensors are sufficient to enable the landing accuracy required or if additional navigation aids such as surface or orbiting beacons will be needed. This study evaluates the system performance requirements to meet the desired landing accuracy for the reference vehicle design and entry, descent, and landing concept of operations. A detailed six degree-of-freedom integrated performance simulation framework is used to perform the assessment and demonstrate that under current assumptions, onboard navigation sensors are sufficient to support precision landing.

#### I. Introduction

Crewed missions to Mars have been the subject of NASA studies for decades, with the latest Design Reference Architecture published in 2009 [1]. More recently, NASA has investigated increasingly detailed entry, descent, and landing (EDL) concepts of operation for this type of mission [2, 3, 4, 5, 6, 7, 8]. In considering the need for multiple landers for logistics and habitats, these studies have highlighted the need for an autonomous safe and precise landing capability on the order of 50 m. Additionally, human-scale missions to Mars will have payload and mass requirements

1

<sup>&</sup>lt;sup>1</sup> Aerospace Engineer, Atmospheric Flight and Entry Systems Branch, AIAA Member.

<sup>&</sup>lt;sup>2</sup> Aerospace Engineer, Atmospheric Flight and Entry Systems Branch, AIAA Associate Fellow.

<sup>&</sup>lt;sup>3</sup> Research Computer Scientist, Atmospheric Flight and Entry Systems Branch.

<sup>&</sup>lt;sup>4</sup> Aerospace Engineer, Atmospheric Flight and Entry Systems Branch, AIAA Senior Member.

<sup>&</sup>lt;sup>5</sup> Aerospace Engineer, Atmospheric Flight and Entry Systems Branch, AIAA Fellow.

<sup>&</sup>lt;sup>6</sup> Member of Technical Staff, Guidance and Control Section.

that are orders of magnitude higher than previous robotic missions such as Mars Science Laboratory (MSL) and Mars 2020. Numerous challenges must be addressed and technologies matured before these types of landings become feasible, including in the areas of spacecraft guidance, navigation, and control (GN&C) [7, 9].

To enable rapid assessment of the various EDL systems in an integrated sense, the Safe and Precise Landing Integrated Capabilities Evolution (SPLICE) project has supported the development of a detailed six degree-of-freedom (6DOF) integrated flight dynamics and GN&C simulation framework based on the Program to Optimize Simulated Trajectories II (POST2) [10]. SPLICE uses this simulation framework to identify key EDL systems that require an increase in technology readiness level (TRL) to enable human-scale Mars landings by evaluating different GN&C systems their effects on overall system performance.

In this work, the integrated performance simulation framework described in [10] and more recently updated in [11] is used to model the reference human-scale low lift-to-drag (L/D) Mars lander described in [8]. Multiple trade studies are carried out to characterize the vehicle and navigation performance using different sets of navigation sensors with varying quality.

#### A. Definitions

Consider a simulation analysis of a spacecraft attempting to reach a target. The truth state dispersion is the collection of the true spacecraft states at a given time or event such as touchdown. The navigation state dispersion is the collection of the navigated spacecraft states as computed by the onboard navigation filter at that corresponding time or event. In the present work, the navigation error is defined to be the difference between the true state and the navigation state, computed as the root-sum-squared (RSS) of the difference between the truth and navigation state vectors. These parameters are illustrated in Fig. 1.

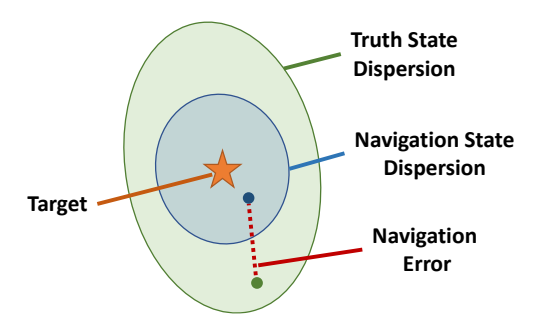


Fig. 1 Dispersion and error definition.

## B. Low L/D Vehicle

NASA-led studies have coalesced around human-scale Mars EDL reference architectures that utilize mid and low L/D entry systems [6, 7, 8]. The present analysis will focus on the low L/D lander that utilizes an inflatable aerodynamic decelerator with aerodynamic flaps [8]. Fig. 2 shows a representation of the entry vehicle with flaps deployed. Table 1 lists relevant vehicle information and assumptions.

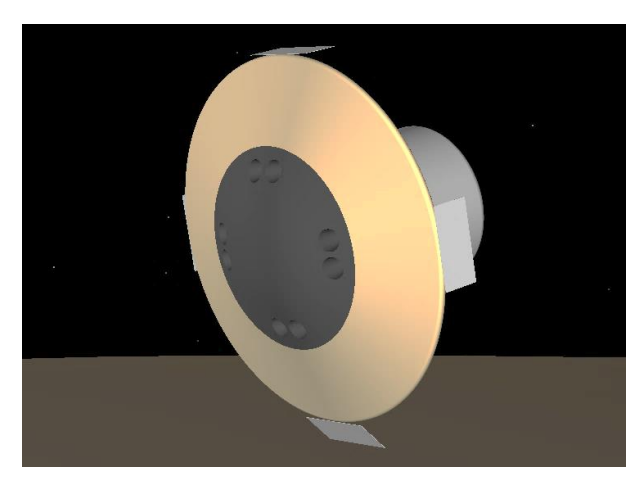


Fig. 2 Representation of the low L/D Mars entry vehicle.

Table 1 Low L/D EDL vehicle information.

System	Parameter	Value / Description	
Mass (Prior to DOI)	Mass	33,151 kg	
Mass (Frior to DOI)	Propellant Load	14,425 kg	
Propulsion	Main Engines (Powered Descent)	8x 100 kN @ 360 s Isp	
r i opuision	RCS (3-Axis On-Orbit; Roll during EDL)	16x 1,000 lbf @ 325 s Isp	
Entry Decelerator	Hypersonic Inflatable Aerodynamic Decelerator (HIAD)	16.4 m diameter	
Entry Control Effector	Aerodynamic Flaps	Four flaps, 3% surface area each, 18°/s actuation rate	
<b>Powered Descent Control Effector</b>	Main Engine Differential Throttling	Nominal thrust 80%	

#### C. Concept of Operations

The low L/D entry vehicle performs the deorbit insertion (DOI) burn using the reaction control system (RCS) at apoapsis of a 1-Sol polar orbit (33793 km apoapsis altitude by 250 km periapsis altitude). The vehicle then coasts for approximately 13 hours until atmospheric entry interface (EI), defined as 125 km altitude. The entry guidance and control algorithms are activated when the sensed vehicle acceleration reaches 0.15 g's (this period between 125 km and 0.15 g's will also be referred to as entry interface in some figures). Throughout entry, the aerodynamic flaps are used for direct force control (DFC), with the guidance commanding angles of attack and sideslip to control downrange and crossrange errors, respectively [12]. At powered descent (PD) initiation (PDI), the supersonic retropropulsion (SRP) main engines are activated, and the vehicle begins the PD main phase using a gravity turn with differentially throttled main engines. During this phase, the gravity turn is augmented with small angles of attack and sideslip (less than approximately 10°) determined by the guidance to take out additional range errors accumulated during atmospheric flight [14]. An intermediate phase occurs near the end of the PD main phase in which the engines are throttle down to achieve a vertical attitude. The PD terminal phase occurs when the vehicle is directly over the landing site and descends vertically with a constant velocity of 2.5 m/s for 5 s. Fig. 3 shows an illustration of each phase of the human-scale low L/D lander concept of operations.

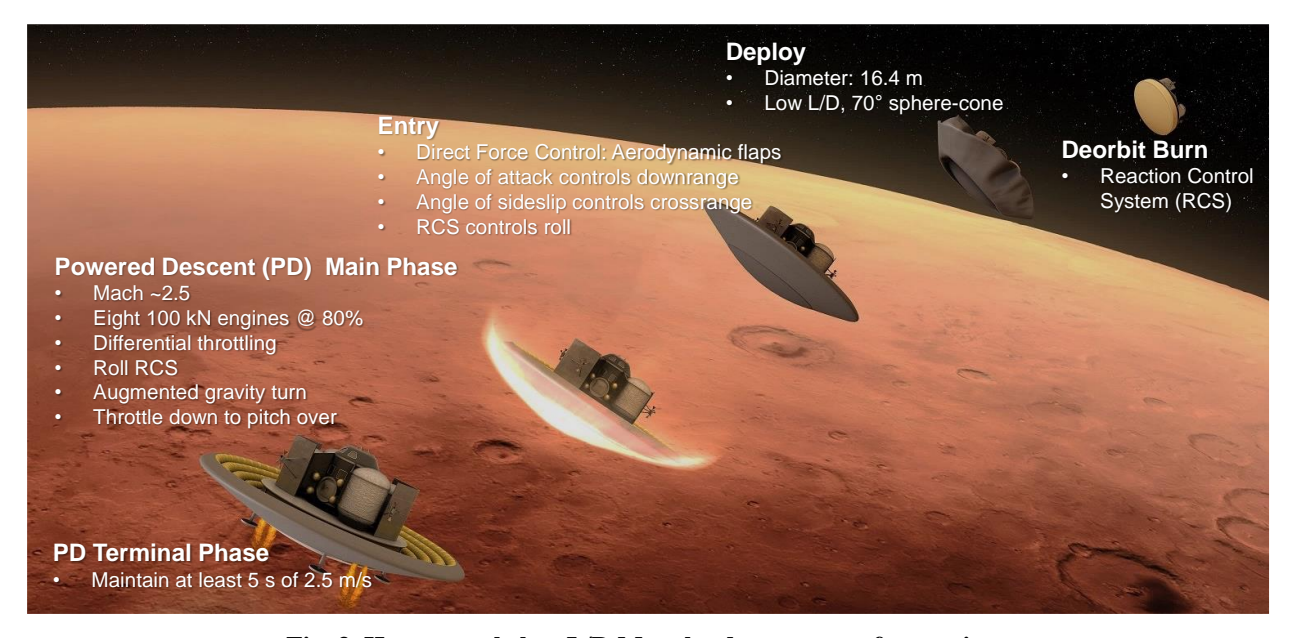


Fig. 3 Human-scale low L/D Mars lander concept of operations.

## II. EDL Integrated System Simulation & Modeling

The EDL case study described in Section I is simulated using the Program to Optimize Simulated Trajectories II (POST2) 6DOF framework originally presented in [10] and updated in [11]. This framework consists of generalized, modular, and user-configurable engineering models of various vehicle systems and environment. For this study, SRP aerodynamic interference effects are neglected.

The overall GN&C system model architecture is the same as that in [11]. Sensor measurements are derived from simulation truth states in the respective sensor models. The outputs of the navigation system, in the form of estimated vehicle states, attitudes, and associated derived quantities, are then passed to the guidance, which determines the necessary vehicle attitude and thrust commands to achieve the desired final state. These commands are passed to the vehicle controllers, which compute the necessary actuator and engine states to achieve those commands. Finally, these states are passed to the vehicle aerodynamic actuators and propulsion systems to impart forces and moments on the vehicle.

## A. Guidance and Control

The guidance and control laws and related systems active during simulated major trajectory phases are shown in Fig. 4. During deorbit and coast phases, open-loop steering laws are used, including attitude station keeping during coasts and a velocity-relative pointing command during the deorbit burn. Closed-loop attitude control is provided by RCS thrusters. A generalized three-axis phase-plane controller [13] directs RCS jet firings to minimize the errors between the commanded and navigated attitude and attitude rates. This algorithm is also used during the initial entry phase prior to the vehicle reaching the sensible atmosphere.

	Loiter Deorbit Coast Entry Interface	Entry	Powered Descent	Vertical Descent	
Propulsion	RCS		Main Engi	nes & RCS	
Guidance	Open-Loop	NPCG			
Steering Law	Attitude Hold	DFC	Augmented Gravity Turn	Vertical	
Roll Control	RCS				
Pitch/Alpha, Yaw/Beta Control	RCS Aerodynamic Differential Throt			Throttling	
RCS Control Law	Phase-Plane				

Fig. 4 Guidance and control laws per major trajectory phase.

A generalized numerical predictor-corrector targeting guidance (NPCG) described in [14] is used for the entirety of EDL. The entry guidance law is direct force control (DFC) using planet-relative angle of attack and sideslip angles to manage downrange and crossrange errors respectively. The powered descent guidance law is an augmented gravity turn. During powered descent, RCS is used for roll (rotation about vehicle axis of symmetry, see Fig. 2 and Fig. 6) control only using the same phase-plane controller. Pitch and yaw control are provided by the eight main engines using differential throttling.

During EDL, the guidance is continuously attempting to target the desired landing site. The guidance will continue to do so even if navigation updates cause the guidance to issue commands that exceed the control authority of the vehicle. The guidance currently does not permit a safe divert, so these situations typically result in the vehicle failing to reach the target and impacting the terrain prior to the start of vertical descent. This is the primary cause of failed cases, as will be shown later in Section IV. Later studies will include assessment of hazard detection sensors and hazard avoidance guidance logic.

# **B.** Navigation

The simulation framework includes a suite of spacecraft navigation models that are generalized to the extent that they can be used to simulate sensors of varying quality for a variety of mission scenarios. The full sensor suite is described in [10] and more recent updates are described in [11]. It includes engineering and behavioral models of an IMU, star tracker, altimeter, velocimeter, navigational Doppler light detection and ranging (LIDAR, NDL), terrain-relative navigation (NDL), hazard detection (HD), and an Earth-based ground/Deep Space Network (DSN) update. This section will summarize the relevant model updates from [11].

For the purposes of the present study, the SPLICE approach to categorizing sensor models is used, in which the *model fidelity* refers to the level of detail the underlying physical and mechanical processes of the sensor that are captured in the model, and *sensor quality* refers to how accurately the sensor measurements reflect truth.

## 1. Sensor Concept of Operations and Assumptions

Fig. 5 shows which sensors are used during different trajectory phases for the concept of operations shown in Fig. 3. Dark gray bars indicate the sensor on that row is inactive. Inertial measurement unit (IMU) measurements are made

continuously throughout all phases of flight using a strapdown IMU model. During the DOI burn and powered descent, all IMU measurements are processed by the navigation filter. During coast phases, only measurements above a specified threshold are processed (see list of assumptions below and Table 2). Star tracker measurements occur during on-orbit loiter and coast phases and terminate 10 minutes prior to the start of entry interface (measurements are not made during DOI burn or EDL). The star tracker model is of low fidelity and simply applies an error model to truth attitude measurements. A Deep Space Network (DSN) state update is made five minutes prior to the deorbit burn, and a second DSN update is made five minutes prior to EI. TRN measurements begin prior to powered descent and end prior to vertical descent using a medium-fidelity sensor model based in part on the Mars 2020 Lander Vision System [11, 15, 16]. Navigational Doppler LIDAR (NDL) measurements are made during the latter phases of powered flight [11, 17, 18]. See Table 2 for TRN and NDL operational ranges. The sensor measurements are ingested by an extended Kalman filter (EKF) provided by the NASA Engineering & Safety Center (NESC) [19]. For this study, the filter process noise only considered noise effects from IMU measurements.

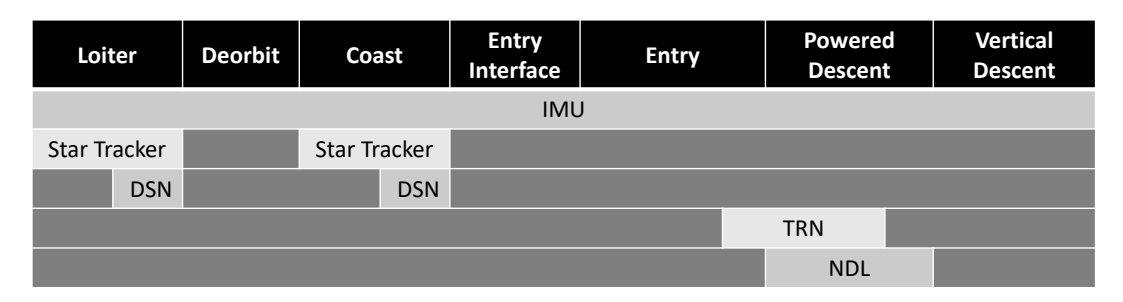


Fig. 5 Navigation sensor concepts of operation.

Several assumptions were made in the implementation and use of the navigation sensors. These are identical to the assumptions in [11]:

- All sensors are mounted perfectly to the rigid body with known alignments (i.e., no sensor-to-body frame misalignments).
- The IMU is calibrated during an unmodeled on-orbit quiescent period, resulting in a reduction of the scale factor and biases by a factor of 10 for the remainder of the flight.
- IMU measurements below the thresholds listed in Table 2 are rejected by the navigation filter to avoid integrating noise. This measurement rejection occurs only during the loiter and coast phases.
- IMU measurements are not quantized.
- The navigation filter process noise includes IMU-related noise only.
- The DSN update is treated as a filter re-initialization rather than a measurement. This means that the DSN state measurement and associated covariance replaces the current filter state and covariance.
- Estimated vehicle mass properties (mass, inertias, and center of gravity location) are obtained directly from the simulation truth values.
- Lag time between sensor measurements and filter processing is unmodeled.
- Spacecraft clock time is the same as the simulation truth time.
- The target landing site (i.e., latitude, longitude, altitude) is known perfectly.

These assumptions must be reevaluated for each new vehicle design and concept of operations, updated as designs mature, and additional data are made available. Including the additional fidelity associated with these assumptions will likely increase the navigation error. Therefore, the results presented herein are not conservative.

#### 2. Sensor Performance Parameters

A summary of the sensor performance parameters is listed in Table 2 and are adapted from various sources. The star tracker and DSN models are of low fidelity since they are simply corrupted truth values using the dispersions in Table 5. Only a subset of the NDL parameters is listed to protect the sensitive nature of some specific performance values.

Table 2 Nominal sensor performance parameters.

Sensor	Parameter	Value	
	Quality	High	
IMU [7]	Measurement Frequency	200 Hz	
	Measurement Threshold Variance	1e-5 m/s, 1e-6 rad	
	Quality	High	
	Measurement Frequency	1 Hz	
	Operational Range	6.0-1.5 km altitude	
	Field of View	90°	
	Number of Maps	4	
TDN [15 17]	Observable Landmarks	100	
TRN [15, 16]	Landmark Bias	1.1x map resolution	
	Camera Pointing Knowledge Error	0.5° 3σ	
	Image Matching Failure	6.6%	
	Camera Focal Length	0.006 m	
	Minimum Map Resolution	1 m/pixel	
	Pixels Per Axis	1024	
NIDI [17 10]	Operational Range	3.0-0.03 km altitude	
NDL [17, 18]	Measurement Frequency	20 Hz	
Star Tracker [7]	Measurement Frequency	0.1 Hz	

#### 3. Vehicle Accommodation

Past studies that evaluated EDL navigation errors for human-scale Mars missions made no assumptions for vehicle accommodation of the sensors. A challenge imposed by the low L/D vehicle relates to how navigation sensors that rely on line-of-sight (LOS) access to the surface are mounted and oriented on the vehicle with a 16 m diameter forebody. Specifically, the deployed HIAD obstructs a significant portion of the payload. Mounting these sensors to the rigid heatshield may be possible, but will require measurement-transparent windows, and SRP plumes may obstruct LOS. Mounting the sensors to the HIAD poses packaging challenges when stowed, uncertainty in sensor location and body-relative orientation, and electrical wiring placement when deployed. Additionally, the level of fidelity of the TRN and NDL models used in this study is such that the camera and beam mounting locations and directions are specified, though do not account for LOS obstructions from the spacecraft outer mold line (OML). Contrast this with a low-fidelity model that might assume the camera or beam is always pointed nadir and does not account for the planet-relative vehicle attitude.

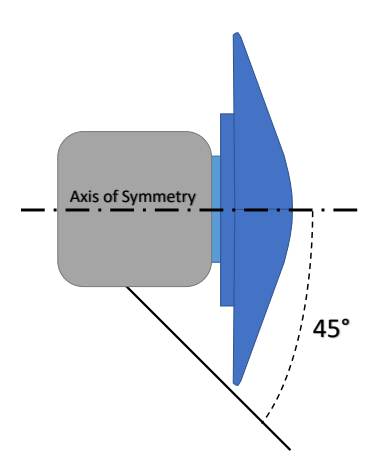


Fig. 6 Vehicle accommodation considerations for LOS-based navigation sensors.

Fig. 6 notionally illustrates how these sensors may be mounted to the vehicle. Using simplified geometry from the depiction in Fig. 2, mounting sensors to approximately halfway up the notional payload OML permits 45° angle of separation from the vehicle centerline, which is suitable for NDL beams that offer better performance when angled close to the vehicle velocity vector. The TRN camera, assuming a 90° field of view, would essentially require mounting to perpendicular to the axis of symmetry if placed on the payload OML.

For this study, the TRN and NDL camera and beam origins are chosen to be embedded in the vehicle heat shield near the centerline. The TRN camera boresight is angled 45° away from the centerline towards nadir if the vehicle

were in steady level flight. The three NDL beams are angled such that they are 45° away from the vehicle centerline, and 120° from each other. While these locations and orientations do not mitigate the mounting challenges particular to this vehicle, they serve to inform the current performance baseline. Future studies will focus on accommodation using refined vehicle OMLs, as well as FOV and mounting location/angle trades.

#### III. Trade Studies

The simulation framework allows the trade of sensor combinations and qualities. The various trade studies that are the focus of this paper are listed in Table 3. The initial objective was to determine if high quality sensor settings were adequate to meet the 50 m landing accuracy requirement (Trade ID #2, uses the sensor schedule shown in Fig. 5) compared to the perfect navigation assumptions made in past studies (ID #1). The perfect navigation case, in which the vehicle GN&C was provided truth simulation data rather than navigation estimates, was run as a basis of comparison. Next, a series of trades assessing the effects of only modifying DSN update quality were run (recall that in this study, the DSN update is treated as a filter reinitialization) to determine the impact of landing and vehicle performance on the reliance on Earth-based updates (Trade IDs #3-6). Finally, a series of trades assessing the effects of the on-board ground-relative sensors (TRN and NDL) were run. This final series of trades identify the quality of onboard sensors required to achieve the precision landing requirements (Trade IDs #7-10).

Category	Trade ID	Trade	Plot Label	DSN (Pre-DOI)	DSN (Pre-EI)	TRN	NDL
Dogolino	1	Perfect Navigation	Perfect Nav	None	None	None	None
Baseline	2	High DSN Updates	Hi DSNs	High	High	High	Yes
Baseline DSN Trades	3	Single DSN Update	Single DSN	High	None	High	Yes
	4	Medium DSN Updates	Med DSN	Medium	Medium	High	Yes
	5	Ultra DSN Updates	Ult DSN	Ultra	Ultra	High	Yes
	6	Low 2nd DSN Update	Low 2nd DSN	High	Low	High	Yes

Med TRN

Med TRN No NDL

Low TRN

Low TRN No NDL

High

High

High

High

High

High

High

High

Medium

Medium

Low

Low

Yes

None

Yes

None

Table 3 Trade Matrix. All runs include a high-quality IMU and high-quality star tracker.

## A. Monte Carlo Dispersions

Ground-

Relative

Sensor

**Trades** 

7

8

9

10

Medium TRN

Medium TRN, No NDL

Low TRN

Low TRN, No NDL

Varying key vehicle design parameters permits evaluation of the robustness of the integrated vehicle systems while providing an assessment of overall vehicle performance for each trade study. Vehicle parameters varied for these trade studies are listed in Table 4 and are derived from previous studies [5, 6, 8, 10, 14]. Specific navigation sensor dispersions obtained from [10] are listed in Table 5. Sensor quality parameters specific to trade studies are listed in Table 6. Dispersions listed as single values apply to all three axes. DSN measurement uncertainties are provided in a velocity-relative u-v-w frame. Monte Carlo analyses consisting of 8,000 distinct trajectories (i.e., samples) were performed for each trade study.

Table 4 Monte Carlo Dispersions. Dispersions listed as triplets refer to X/Y/Z axes unless otherwise noted.

Category	Parameter	Dispersion	Distribution
	Body Rates	0.3°/s 3σ	normal
Initial Conditions	Attitude (Velocity-relative)	$3.0^{\circ}~3\sigma$	normal
	Uncorrelated state covariance	$0.03^{\circ} 3\sigma$ for angles, $0.03 \text{ km } 3\sigma$ for altitudes	normal
	Peak thrust	Scale factor: 1% $3\sigma$	normal
	Peak Isp	Scale factor: 1% $3\sigma$	normal
Propulsion	Start lag time	0.0:0.2 s	uniform
	Startup transient rate	Scale factor: 1% $3\sigma$	normal
	Main phase response rate	Scale factor: 1% $3\sigma$	normal
	Mass	$250~{ m kg}~3\sigma$	normal
Mass	Center of gravity	$0.05 / 0.01 / 0.01 \text{ m } 3\sigma$	normal
	Moments of inertia	$1\% \text{ kg-m}^2 3\sigma$	normal

Table 5 Navigation sensor dispersions [10]. Dispersions listed as single values apply to all three axes. Dispersions listed as triplets refer to X/Y/Z axes unless otherwise noted.

Sensor	Parameter	Dispersion (X/Y/Z Axes)	Distribution		
	Accelerometer Misalignment	17 arcsec $3\sigma$	normal		
	Accelerometer Scale Factor	$450~\mathrm{ppm}~3\sigma$	normal		
	Accelerometer Bias	84 micro-g $3\sigma$	normal		
IMIT	Accelerometer Velocity Random Walk	$0.003 \text{ m/s}^2 3\sigma$	normal		
IMU	Gyroscope Misalignment	19 arcsec $3\sigma$	normal		
	Gyroscope Scale Factor	$27 \text{ ppm } 3\sigma$	normal		
	Gyroscope Bias	$0.036$ °/hr $3\sigma$	normal		
	Gyroscope Angular Random Walk	$0.015~^{\circ}/\sqrt{\mathrm{hr}~3\sigma}$	normal		
Cton Tue alson	Misalignment	8 arcsec $3\sigma$	normal		
Star Tracker	Boresight Noise	24 arcsec $3\sigma$	normal		
DON H. J. A.	Position Bias (u-v-w frame)	$500 / 1000 / 200 \text{ m } 3\sigma$	normal		
DSN Update	Velocity Bias (u-v-w frame)	$0.05$ / $0.10$ / $0.01$ m/s $3\sigma$	normal		
NDL	NDL Error Model				
Optical TRN	See TRN sensor specifications in Table 2				

Table 6 Sensor quality parameters.

Sensor	Parameter ↓ (	Quality →	Low	Medium	High	Ultra
	Position Bias (u-v-w fram	ie, m, 3σ	4500 / 7500 /	3000 / 5000 /	500 / 1000 /	50 / 100 /
DSN	normal)		1500	1000	200	20
DSN	Velocity Bias (u-v-w fran	ne, m/s, $3\sigma$	0.15 / 0.30 /	0.10 / 0.20 /	0.05 / 0.10 /	0.005 / 0.010 /
	normal)		0.08	0.05	0.01	0.001
	Number of Maps		1	2	4	N/A
	Minimum Altitude, m		1500	1000	500	N/A
Ontical	Observable Landmarks		25	50	100	N/A
Optical TRN	Map Accuracy Scale Fact	or	1.3	1.2	1.1	N/A
	Camera focal length unce	rtainty	0.6%	0.5%	0.4%	N/A
	Camera orientation uncertainty, deg,		0.75	0.50	0.25	N/A
	$3\sigma$ normal	$\sigma$ normal		0.30	0.23	1 <b>N</b> /A

## **B.** Performance Metrics

While the integrated performance simulation framework permits the assessment of a wide variety performance parameters, the present study will focus on those related to navigation:

- 1. *Navigation error:* This parameter describes the overall behavior of the navigation system. Specifically, the navigation errors at specific events are assessed to understand how the various navigation sensors, when activated and deactivated, affect the evolution of the navigation error.
- 2. Landing precision: This parameter describes how well the integrated vehicle lands near the pre-designated target. Currently, a landing precision (i.e., range to target at touchdown) of 50 m in a  $3\sigma$  sense is desired. For this analysis, it is assumed that the inertial location of the landing site is known perfectly (e.g., is not dispersed), and that the same location is used for GN&C targeting. The present study will also assess landing precision in a 99%-tile sense to better capture the effects of outliers.
- 3. Success rate: The success rate describes the percentage of 8,000 Monte Carlo samples that achieve a safe (or successful) landing. The present study defines a safe landing as one that reaches the touchdown event with a horizontal (translational) velocity of less than or equal to 1.0 m/s, a vertical velocity of less than 3.0 m/s, an angle off vertical of less than 3°, and a maximum angular rate about any axis of less than 0.5°/s. A success rate of 99% or better is desired.

An exception to the above performance metrics relates to the roll rate at touchdown. Excessive roll rates were observed at the start of vertical descent and increasing towards touchdown. This effect is unlikely to be a physical phenomenon unique to this vehicle design and is expected to be mitigated through more rigorous RCS controller tuning. All trades in this paper include this behavior, but since it did not adversely affect performance, the roll rate constraint was not applied in filtering the success rate.

#### IV. Results

Results from the POST2 simulations of the human-scale Mars lander described in Section I using the simulation framework, models, and assumptions described in Sections II and III are presented here. Recall from Section II that the guidance used in this study is designed to target the desired landing site and does not permit a safe divert. Lack of a safe divert mode means that the guidance will attempt to fly the vehicle to the landing site, even if control authority is exceeded. This behavior is typically the primary cause of failed dispersed trajectories.

#### A. Baseline Cases

Until now, human Mars EDL studies have assumed perfect navigation (guidance and control receive perfect state information from the truth simulation) and therefore, provide a theoretical best case. Consider first range to the landing target at touchdown. Fig. 7 provides the statistics for range at touchdown using perfect navigation and shows that, with 100% success (rounded to the nearest tenth of a percent), the 99%-tile is approximately 43 m. This range statistic is within the requirement of 50 m but leaves little margin for navigation errors or the impacts of the assumptions listed in Section II.B. Fig. 7 also provides, in the upper left plot, a histogram of the perfect navigation ("Perfect Nav") results in blue, and in the plot on the right, the quantile-quantile plot in blue along with the dashed blue line denoting a gaussian distribution. Note that the results are mostly gaussian until the range reaches approximately 25 m from the target.

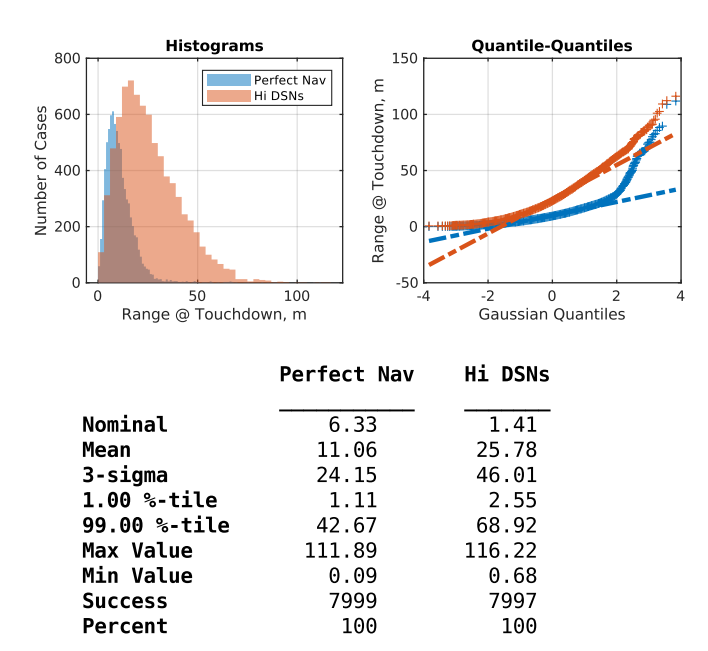


Fig. 7 Landing precision statistics (meters), baseline trades. Note that the listed percent success rate is rounded to the nearest tenth of a percent.

These results are then compared to the case that includes navigation errors using the two high quality DSN updates (defined in Table 3 as Trade ID #2 and labeled "High DSNs"), the success rate remains high at 100%. However, the 99%-tile range at touchdown increases by over 50% to 68.92 m 99%-tile, exceeding the 50 m landing requirement. The histogram and quantile-quantile are shown (in red) for comparison to the perfect navigation case in Fig. 7. Addressing this increase in range at touchdown and increasing the precision back down to below 50 m remains a challenge, which will be discussed later in this paper. If landing accuracies of 100 m were to be deemed adequate for human Mars missions, then the "Hi DSNs" configuration offers some margin to the limit.

A second metric of importance for Mars EDL missions is propellant used during EDL, shown in Fig. 8 for the same two cases. The EDL propellent used includes all propellant expended during RCS and main engine firings from EI to touchdown. While including the navigation errors increases the range at touchdown in the "Hi DSNs" case, these errors do not have a significant impact on the 99%-tile propellant use (less than 100 kg 99%-tile increase). The focus of the present study is navigation performance, but this metric is included to provide an example of benefits of a multidisciplinary integrated performance simulation capability to evaluate navigation impact on various subsystems.

In summary, the result of the baseline comparisons show that the high-quality navigation sensors alone are not sufficient to meet the 50 m landing accuracy requirement, but do enable a satisfactory (99% or more) success rate.

Therefore, subsequent trades consider the effectiveness of additional variations in DSN and TRN sensor quality to reduce range at touchdown.

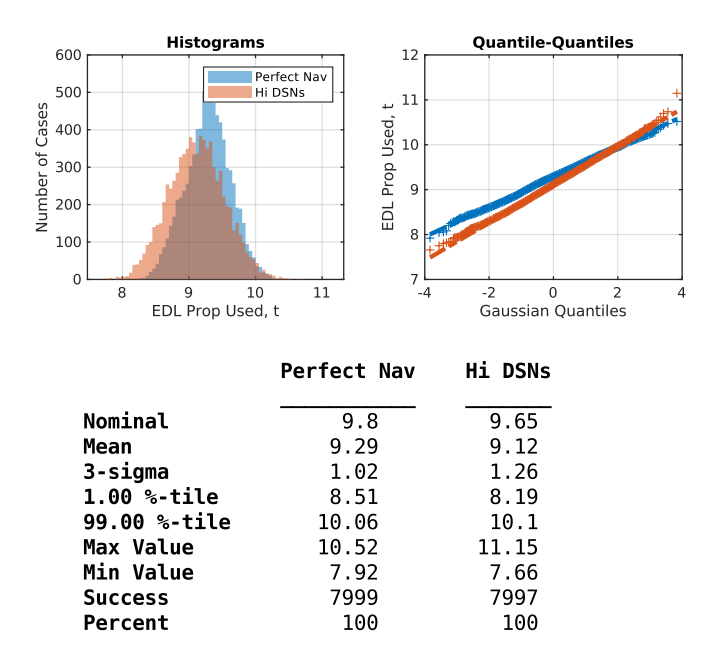


Fig. 8 EDL propellant consumed statistics (metric tons), baseline trades.

#### **B. DSN Trades**

Trades were performed to study the effects of DSN update quality on integrated performance. These cases considered circumstances where a data dropout might result in worse state update quality as well as the availability of additional tracking assets that could provide navigation updates better than the assumed DSN high quality update. Therefore, four additional cases were considered. The dual (five minutes prior to both DOI and EI) high-quality DSN filter reinitialization case from the baseline trades is included here as a basis of comparison, labeled "Hi DSNs." A case with only a single high quality DSN filter reinitialization made prior to DOI is considered and labeled "Single DSN." A case with two DSN filter reinitializations at the same times as that of the baseline High DSNs trade, but of medium quality, is considered and labeled "Med DSNs." Both cases were expected to produce larger ranges at touchdown compared to the baseline, so another case explored an improved DSN update using two DSN filter reinitializations of "ultra high" quality that reduced the errors of the baseline case by a factor of ten. While this level of improvement is possibly unrealistic, it was chosen to characterize performance as close-to-perfect state knowledge is approached. This case is labeled "Ult DSNs." Finally, another case is considered that assumes a high quality DSN filter reinitialization prior to DOI but only a low quality DSN filter reinitialization prior to EI is labeled "Low 2nd DSN." The specific values used for these various DSN qualities are listed in Table 6.

Fig. 9 shows the landing precision metric (range at touchdown) for the five DSN trades. It can immediately be seen that a single DSN filter reinitialization prior to DOI (denoted in red as "Single DSN") results in unacceptable precision (1800 m 99%-tile) and a poor success rate (46%). Put another way, this case results in both unsafe and imprecise landing. Therefore, a single DSN update prior to DOI is insufficient to meet the landing requirement without the use of additional onboard sensor capability beyond the included high-quality IMU, TRN, and NDL, or offboard systems such as navigation beacons.

The next trade, considering medium quality DSN filter reinitialization before DOI and PDI (denoted in yellow as "Med DSNs") also shows unacceptable performance as expected, though not as poor as with a single reinitialization. Like the previous case, this configuration would need to rely on additional capability beyond the baseline high quality sensor suite to improve performance to meet the 50 m requirement.

DSN filter reinitializations of superior ("ultra") quality, ten times better than the baseline, shows that the landing precision requirement of 50 m can be reached with a 100% success rate. When comparing this case to the Perfect Navigation case from Fig. 6, this case demonstrates the limit on DSN to achieve the 50 m navigation accuracy. While DSN measurements of this accuracy are likely unrealistic, this case does demonstrate that the performance metrics can be met with sufficiently accurate ground tracking data, or some method of improving state knowledge prior to EI

such as high-altitude TRN. The investments to achieve the increased accuracy need to be weighed against other improvements to onboard sensors and/or offboard methods such as beacons.

The final case with a DSN filter reinitialization of low quality prior to EI shows performance comparable to the two medium quality DSN filter reinitializations, which emphasizes the need for ground tracking measurements made as late and as accurate as possible. No considerations were made in this study to account for time needed to track, calculate, and transmit the filter reinitialization state, which may be different between 1 Sol and 5 Sol orbits.

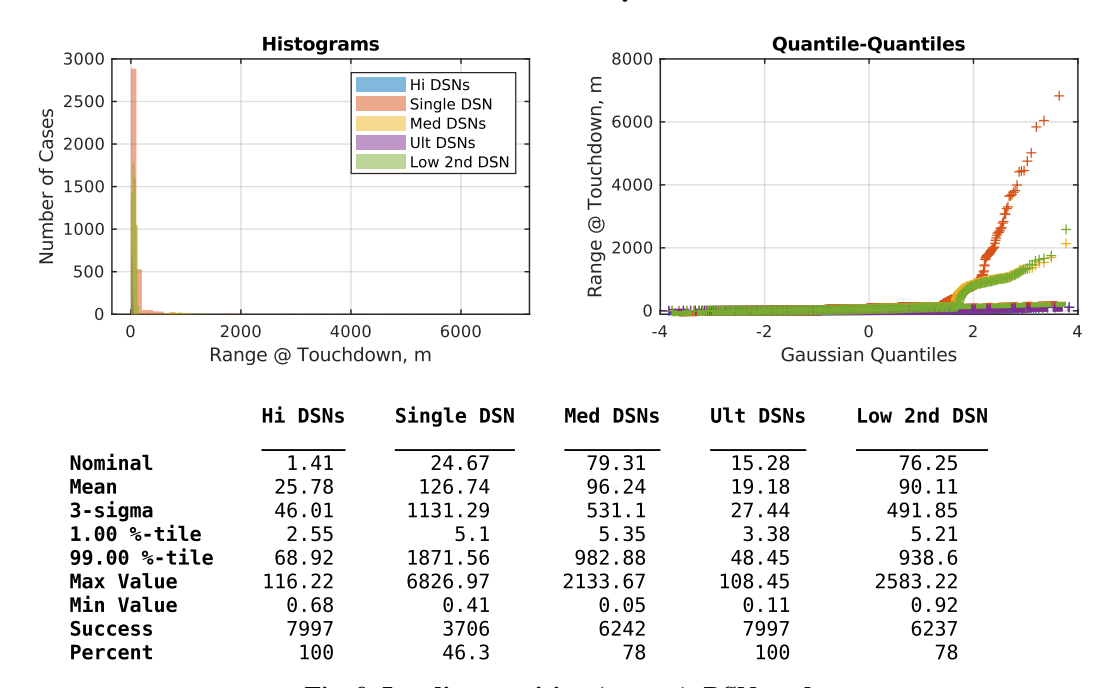


Fig. 9 Landing precision (meters), DSN trades.

Fig. 10 shows the navigation position error at EI and Fig. 11 shows the final navigation position error at touchdown for the five DSN trades. These results illustrate how the navigation position error evolves between EI and touchdown. Recall from Fig. 1 that the navigation error is defined in this study as the RMS of the difference between the truth and onboard state estimates. Both the dual high-quality DSN and dual ultra-quality DSN cases show less than 1.0 km errors at EI (99%-tile), while all other cases show errors on the order of 3-4 km. These latter cases also show unacceptable success rates (78% or less).

In Fig. 10 s, the "High DSNs" case shows an 878 m 99%-tile error at EI. The second case, "Single DSN," removes the second high-quality DSN update prior to EI that occurs after a 13 hour coast phase from apoapsis. Removing that update increases the navigation position error at EI to 4344 m 99%-tile. The medium quality DSN trade, "Med DSNs," still shows poor navigation error, 3380 m 99%-tile. The "Ultra DSNs" trade shows excellent navigation position error of 127 m 99%-tile at EI. Finally, the "Low 2nd DSN" case, which uses a high-quality DSN filter reinitialization prior to DOI and a low-quality DSN filter reinitialization prior to EI, again shows a large navigation position error at EI of 3378 m 99%-tile. Since the implementation of the DSN update for this study forces the navigation filter to replace the portion of the onboard covariance that describes the state with the DSN update covariance, as opposed to treating the DSN update as a measurement, the majority of the performance impact occurs from the second update prior to DOI.

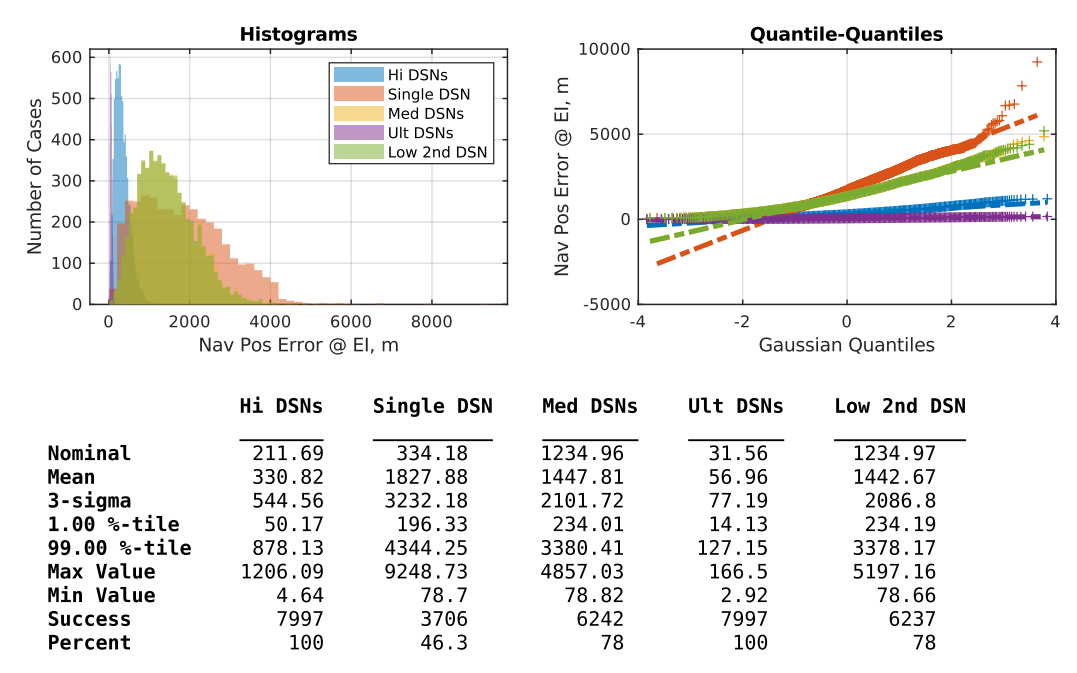


Fig. 10 Navigation position error at EI (meters), DSN trades.

Fig. 11 shows that despite the effects of the various DSN updates, the 99%-tile values are essentially unchanged from the baseline "Hi DSNs" case, though there is a minor improvement with the higher DSN update qualities. This similarity indicates that the high-quality ground-relative navigation sensors used in these DSN trades significantly reduce the navigation error during EDL, but do not improve the success rate as the DSN quality varies. There are other ways to improve the guidance ability to clean up outlying points in the medium quality DSN cases, through additional vehicle control or additional propellant, but those options are not considered here. Therefore, reducing the errors at entry interface to less than 1.0 km, however it is achieved, is advantageous to minimize navigation position errors at touchdown with this vehicle guidance and control strategy.

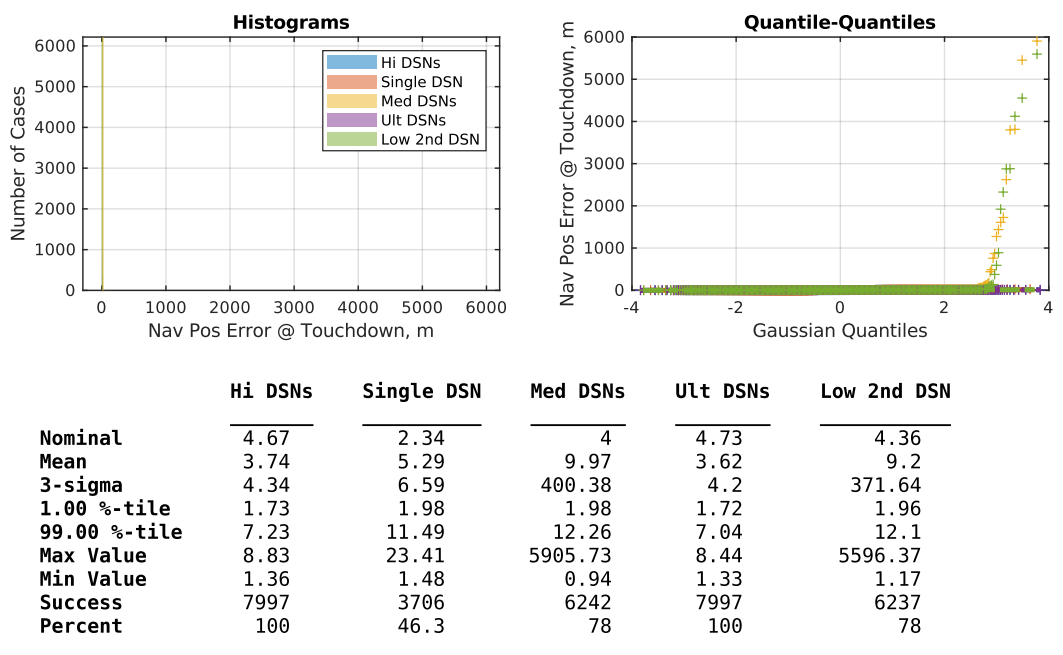


Fig. 11 Navigation position error at touchdown (meters), DSN trades.

## C. Ground-relative Navigation Trades

Trades were performed to study the effects of different ground-relative navigation sensor quality and combinations on navigation performance. These trades all assume the high quality DSN update 5 min prior to DOI and EI. Recall that the baseline navigation-in-the-loop case from the baseline trades also uses a high quality TRN and NDL sensor. This trade evaluates how performance degrades when a lower quality TRN sensor (Med TRN or Low TRN) is used with or without (No NDL) measurements from the lower altitude NDL sensor. The settings for medium and low quality TRN are defined in Table 6.

Though not included here as a plot, the landing precision (range at touchdown) metric for the ground-relative navigation trades are listed in Table 7 and were essentially invariant (approximately 70 m 99%-tile). Using the medium quality TRN with or without NDL did not have a significant effect on success criteria (down to 96.4% from 100%), implying that a medium quality TRN system alone may adequate for a safe landing, at the cost of increased navigation errors. However, if a low quality TRN is used without an NDL sensor, the success rate falls to 22%. This implies that low quality TRN cannot be solely relied upon to reduce navigation errors sufficiently to meet a 50 m landing requirement due in large part to navigation errors. This is shown in the following figure.

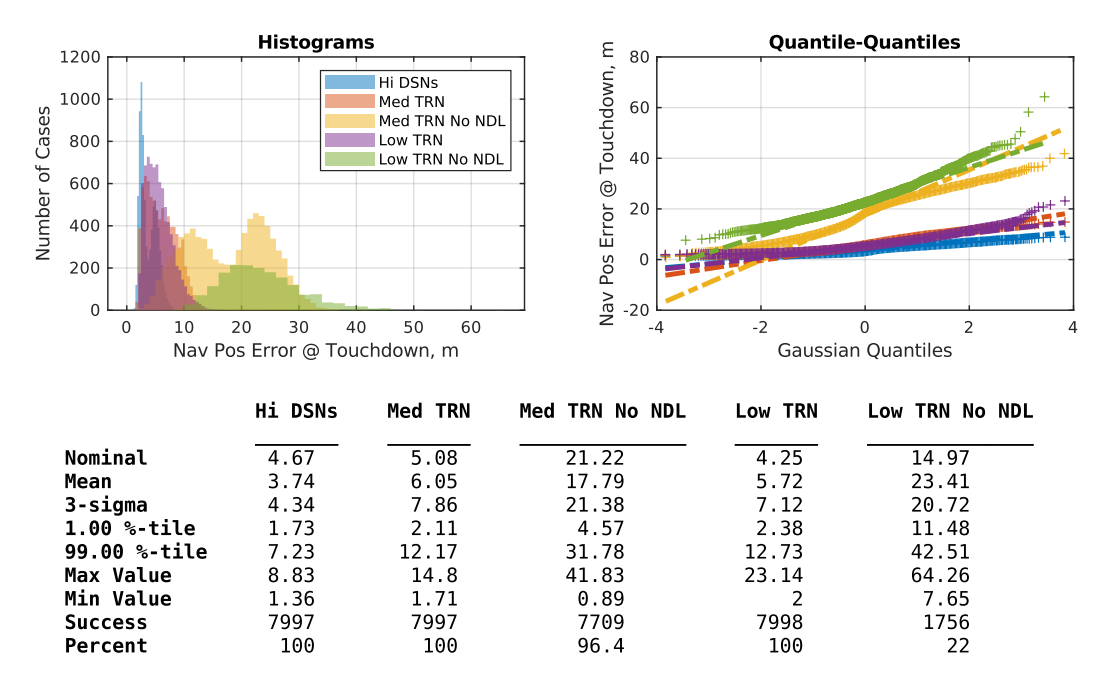


Fig. 12 Navigation position error at touchdown (meters), ground-relative sensor trades.

Fig. 12 shows the navigation position error at touchdown for the ground-relative sensor trades. First, note how the error for both the medium and low quality TRN trades, "Med TRN" and "Low TRN," is essentially the same, approximately 12-13 m 99%-tile, and show high success rates (100%). The similarity in performance may be attributed in part to the NDL sensor being active in both cases. Next, the trade with a medium quality TRN and no NDL sensor, "Med TRN No NDL," initially appears to offer marginal performance (96.4% success rate), but the navigation position error is significantly higher than the cases with NDL (increased to 31.78 m 99%-tile). The error increase is particularly significant since it is approaching the actual touchdown precision landing requirement of 50 m. Finally, the trade with low quality TRN and no NDL shows the worst performance, with only a 22% success rate and 43 m navigation position error. These trades highlight how necessary an NDL-like sensor is needed for safe landing at Mars.

Fig. 13 shows the navigation velocity error at touchdown for the ground-relative sensor trades. While the 99%-tile errors are low overall, the use of the NDL sensor significantly reduces the navigation velocity error. This reduction is an intuitive result since the NDL sensor is designed to provide the navigation filter with an estimate of velocity and range.

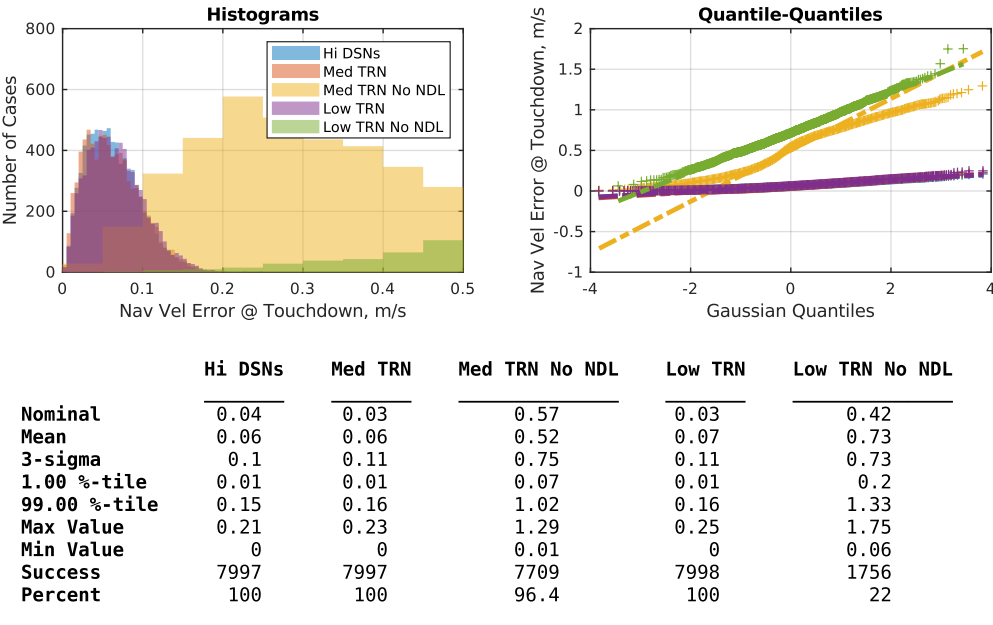


Fig. 13 Navigation velocity errors at touchdown (meters per second), ground-relative sensor trades.

#### D. Summary of Results

A summary of the relevant integrated performance statistics and metrics for all trades are listed in Table 7. Among these, only the case with the ultra-high-quality DSN filter reinitializations met both the safe (greater than 99%) and precise (less than 50 m) landing requirement, though with no margin left in the latter. For trades with greater than 99% success rates, the propellant consumption during EDL was essentially invariant at approximately 10 t. Overall velocity and attitude navigation errors are small, due in large part to the ground-relative sensors during EDL and high-quality star tracker during exoatmospheric coast phases.

	Trade	Success Rate %	Landing Precision 99%-tile, m	EDL Prop Used 99%-tile, t	Nav Pos Err @ TD 99%-tile, m	Nav Vel Err @ TD 99%-tile, m/s	Nav Att Err @ TD 3σ, deg
Baseline	Perfect Navigation High DSN Updates	100.0 100.0	42.67 68.92	10.06 10.10	0.00 7.23	0.00 0.15	0.00 0.21
DSN Trades	Single DSN Update Medium DSN Updates Ultra DSN Updates Low 2nd DSN Update	46.3 78.0 100.0 78.0	1871.56 982.88 48.45 938.60	10.11 12.88 9.93 12.70	11.49 12.26 7.04 12.10	0.22 0.28 0.16 0.28	0.27 0.78 0.19 0.63
Ground- Relative	Medium TRN Medium TRN, No NDL	100.0 96.4	70.25 67.54	10.10 10.19	12.17 31.78	0.16 1.02	0.22 0.03
Sensor Trades	Low TRN Low TRN, No NDL	100.0 22.0	72.44 72.46	10.10 10.09	12.73 42.51	0.16 1.33	0.22 0.02

**Table 7 Integrated performance summary.** 

## V. Conclusions

This study presents the first results of a fully integrated navigation-in-the-loop assessment of landing performance for the low L/D Mars lander used in recent NASA studies of human-scale landings. The DSN and ground-relative sensor trades focused on navigation performance under different sensor assumptions showed that achieving both a safe and precise landing remains a challenge. Improving ground tracking accuracy is one potential method to meet the required precision, and a second DSN filter reinitialization prior to EI is likely required. However, even with perfect navigation assumptions, the landing precision is still very close to 50 m and leaves little margin for additional errors that will be introduced as simulation fidelity and assumptions are improved. Finally, it was shown that the ground-relative navigation sensors offer significant navigation error improvements, though vehicle accommodation

considerations remain. The results presented in this study are highly dependent on the vehicle concept of operations and the assumptions presented, and additional navigation infrastructure (e.g., beacons in orbit or on the surface) cannot be ruled out.

Future work includes assessing the impact of high-altitude TRN measurements on reducing navigation error without the need for unrealistically accurate ground tracking, as well as modeling beam-based (i.e., active rather than passive/optical) TRN sensors. Modeling realistic DSN tracking data for both 1 Sol and 5 Sol orbits will also aid assessment of the level of accuracy available for this type of mission. Additional filter and controller tuning will be required to improve EKF performance and address the excessive roll rates at touchdown. Considerations for hazard detection and avoidance (HDA) sensors, measurement acquisition and processing time, and resultant divert maneuvers will also inform trajectory design. As human-scale Mars vehicle designs mature, sensor models, specifications, and dispersions will be updated within the simulation framework.

## Acknowledgments

The authors thank Eric Queen (LaRC) for RCS phase plane controller design and Chris Karlgaard (AMA) for supporting the implementation and testing of the MEKF in the simulation framework. The authors are also grateful to Scott Striepe (LaRC) for insight and discussions regarding this work. A portion of this research was carried out at the Jet Propulsion Laboratory, California Institute of Technology, under a contract with the National Aeronautics and Space Administration.

## References

- [1] Drake, B. G., "Human Exploration of Mars Design Reference Architecture 5.0," NASA SP-2009-566.
- [2] Craig, D. A., Herrmann, N. B., and Troutman, P. A. "The Evolvable Mars Campaign Study Status," IEEE Aerospace Conference, Big Sky, MT, March 7-14, 2015.
- [3] Cianciolo, A. D. and Polsgrove, T. T., "Human Mars Entry, Descent and Landing Architecture Study Overview," AIAA 2016-5494.
- [4] Cianciolo, A. D. and Polsgrove, T. T., "Human Mars Entry, Descent and Landing Architecture Study: Phase 2 Summary," AIAA 2018-5190.
- [5] Percy, T., Polsgrove, T., Sutherlin, S., and Dwyer-Cianciolo, "Human Mars Entry, Descent, and Landing Architecture Study: Descent Systems," AIAA 2018-5193.
- [6] Dwyer-Cianciolo, A. M., Dillman, R. A., Brune, A. J., Lugo, R. A., Polsgrove, T., Percy, T., Sutherlin, S., and Cassell, A. M., "Human Mars Entry, Descent, and Landing Architecture Study: Deployable Decelerators," AIAA 2018-5191.
- [7] Dwyer-Cianciolo, A. M., Polsgrove, T., Sostaric, R. R., Edquist, K. T., Korzun, A. M., and Garcia, J. A., "Human Mars Entry, Descent, and Landing Architecture Study: Phase 3 Summary," AIAA 2020-1509.
- [8] Cianciolo, A. D., Lugo, R. A., Korzun, A. M., Slagle, A. C., Queen, E. M., Dillman, R. A., and Powell, R. W., "Low Lift-to-Drag Morphing Shape Design," AIAA 2020-1266.
- [9] Cianciolo, A. D., Striepe, S., Carson, J., Sostaric, R., Woffinden, D., Karlgaard, C., Lugo, R., Powell, R., and Tynis, J., "Defining Navigation Requirements for Future Precision Lander Missions," AIAA 2019-0661.
- [10] Cianciolo, A. D., Dutta, S., Lugo, R. A., Williams, R. A., and Chen, P., "A Simulation Framework for Precision Landing and Hazard Avoidance Technology Assessments," AIAA 2020-0366.
- [11] Lugo, R. A., Cianciolo, A. D., Dutta, S., Williams, R. A., Green, J. S., Chen, P., D'Souza, S., and Pensado, A. R., "Precision Landing Performance and Technology Assessments of a Human-Scale Lunar Lander Using a Generalized Simulation Framework," Accepted, AIAA SciTech 2022.
- [12] Cianciolo, A. D., and Powell, R. W., "Entry, Descent, and Landing Guidance and Control Approaches to Satisfy Mars Human Mission Landing Criteria," AAS 17-254.
- [13] Calhoun, P. C., and Queen, E. M., "Entry Vehicle Control System Design for the Mars Smart Lander," AIAA 2002-4504.
- [14] Lugo, R. A., Powell, R. W., and Cianciolo, A. D., "Overview of a Generalized Numerical Predictor-Corrector Targeting Guidance with Application to Human-Scale Mars Entry, Descent, and Landing," AIAA 2020-0846.
- [15] Mourikis, A. I., Trawny, N., Roumeliotis, S. I., Johnson, A. E., Ansar, A., and Matthies, L., "Vision-Aided Inertial Navigation for Spacecraft Entry, Descent, and Landing," IEEE Transactions on Robotics, vol. 25, no. 2, pp. 264-280, 2009.
- [16] Johnson, A., Aaron, S., Chang, J., Cheng, Y., Montgomery, J., Mohan, M., Schroeder, S., Tweddle, B., Trawny, N., and Zheng, J., "The Lander Vision System for Mars 2020 Entry Descent and Landing," Proceedings of the Advances in the Astronautical Science Guidance Navigation and Control, vol. 159, no. 36, 2017.
- [17] Gragossian, A., Pierrottet, D., Estes, J., Barnes, B. W., Amzajerdian, F., and Hines, G. D., "Navigation Doppler Lidar Performance at High Speed and Long Range," AIAA 2020-0369.
- [18] Pierrottet, D. F., Hines, G. D., Barnes, B. W., Amzajerdian, F., Petway, L. B., Carson III, J. M., "Navigation Doppler Lidar Integrated Testing Aboard Autonomous Rocket Powered Vehicles," AIAA 2018-0614.
- [19] Murri, D. G., Striepe, S. A., and Powell, R. W., "NESC Report Assessment #09-00530, Phase 2: Simulation Framework for Rapid Entry, Descent, and Landing (EDL) Analysis," NESC-RP-09-00530. NASA-TM-2011-217063.